Journal of Power Sources 233 (2013) 369–379

Contents lists available at SciVerse ScienceDirect

Journal of Power Sources

journal homepage: www.elsevier.com/locate/jpowsour

# A statistically-based thermal conductivity model for fuel cell Gas Diffusion Layers

Hamidreza Sadeghifar [a,*], Majid Bahrami [a], Ned Djilali [b]

[a] Mechatronic Systems Engineering, School of Engineering Science, Simon Fraser University, Surrey V3T 0A3, BC, Canada
[b] Department of Mechanical Engineering and Institute for Integrated Energy Systems, University of Victoria, Victoria V8W 3P6, BC, Canada

## HIGHLIGHTS

- A statistical model is developed for estimating GDL thermal conductivity.
- The model considers the statistical distribution of GDL geometrical parameters.
- Angle and aspect ratio distributions are measured for some GDLs.
- The dependency of thermal conductivity on geometrical parameters is considered.
- New techniques are introduced for GDL geometrical property measurements.

## GRAPHICAL ABSTRACT

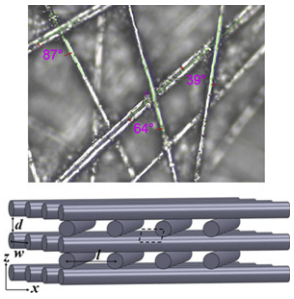


## ARTICLE INFO

*Article history:*
Received 18 October 2012
Received in revised form
17 December 2012
Accepted 16 January 2013
Available online 29 January 2013

*Keywords:*
Thermal conductivity
Porous media
Fibrous media
Gas Diffusion Layer
Angle distribution
Fuel cell

## ABSTRACT

Many of the characterization and theoretical analyses of Gas Diffusion Layers (GDL) transport properties have to date been done as a function of porosity with little attention paid to other geometrical properties. In this paper, a statistical unit cell approach is presented for predicting the thermal conductivity of GDLs by introducing geometrical properties such as the intersecting fiber angles and characteristic distances/aspect ratios. These geometrical properties are deconvoluted analytically using optical and porometry data. The dependency of the thermal conductivity on the geometrical parameters is analyzed, and the GDL structure for optimal heat conduction is identified. It is shown that aspect ratio is as important as porosity in determining conductivity, and that the traditional notion that a porous medium with higher porosity has a lower thermal conductivity is not always true. The maximum thermal conductivity depends primarily on porosity and fiber angle, occurs at an aspect ratio of around unity, and shows negligible dependence on fiber diameter. The geometrical concepts and the measured data presented in this paper help unravel some unexplained trends reported in the literature and provide novel insights on avenues to optimize GDLs. The methodology can be extended to estimate other transport properties such as permeability.



## 1. Introduction

Over the past few years, there has been an increasing interest in using Proton Exchange Membrane Fuel Cells (PEMFCs) as an environmentally friendly power source. Accurate estimation of the temperature distribution and associated heat transfer rates in PEMFCs is essential to quantify various transport phenomena such as water and species transport, reaction kinetics, and rate of phase change [1–4]. A key thermo-physical property for such purpose is the thermal conductivity of the membrane-electrode assembly components, particularly the Gas Diffusion Layer (GDL) [5–9]. The estimation of this property presents a number of challenges, including lack of a detailed understanding of the way heat is transferred in such random micro-structured porous materials,

* Corresponding author. Tel.: +1 (778) 782 8587; fax: +1 (778) 782 7514.
*E-mail addresses:* sadeghif@sfu.ca (H. Sadeghifar), mbahrami@sfu.ca (M. Bahrami), ndjilali@uvic.ca (N. Djilali).

0378-7753/$ – see front matter © 2013 Elsevier B.V. All rights reserved.
http://dx.doi.org/10.1016/j.jpowsour.2013.01.086

and the determination of the geometrical parameters specific to each type of GDL. In parallel with the progress in PEMFC technology, new GDLs with different materials and characteristics are being manufactured for new designs and applications. As a result, measuring the geometrical characteristics of GDLs and developing a general model for predicting their thermal conductivity at different operating conditions is essential for the modeling and design of PEMFCs.

A few analytical models have been presented in the open literature for estimating the through-plane thermal conductivity of GDLs. Most of these models are based on porosity only and do not consider other important geometrical parameters such as fiber angles and aspect ratio, that is, the ratio of the distance between fibers in the in-plane ($x$–$y$) directions. The main idea in these models [10–12] is to construct a porous structure having the same porosity as the actual GDL, and then use a theoretical model to calculate the thermal conductivity on the basis of the solid and pore fractions, i.e., porosity. The results show similar values for thermal conductivity of different GDLs having the same porosity and sometimes overestimate [10] or underestimate [11,12] the measured thermal conductivity. Considering the complexity of the structure of a fibrous porous medium, improvements in model accuracy are likely to require consideration of all salient geometric parameters. In this work, an attempt is made to incorporate the intersecting angle and characteristic distance between fibers into a new analytical model.

The work builds on the unit cell approach of Bahrami et al. [13] (see also [14–18]) that was successfully applied to several heat transfer applications such as packed beds, and of Sadeghi et al. [1] who presented the first analytical model that took the main geometrical parameters into account in modeling GDLs. The focus of the present study will mainly be on introducing new approaches for determining the geometrical parameters of different GDLs and applying the determined parameters to a statistical unit cell approach for the estimation of thermal conductivity. A comprehensive parametric study of the geometrical parameters is performed to investigate their effects on heat transfer and identify the dominant parameters. The results of this study provide detailed information on the thermal conductivity of various types of GDLs. The results are useful for performance modeling and provide novel physical insights that can guide design and manufacturing of GDLs.

## 2. Model development and geometrical data measurements

The temperature field and heat transfer rates in a fibrous porous media depend on a variety of factors including geometrical, material, mechanical, and thermal properties, as well as operating conditions. The structure and thermal conductivity of GDLs is anisotropic, and thus representative geometrical modeling will be important. The focus here is on modeling of the through-plane thermal conductivity, though the presented concept is general and, with some modifications, can be adapted to the estimation of other transport properties such as in-plane thermal conductivity and permeability. In general, the present model is an extension of the previous work of Bahrami and Djilali (model of Sadeghi et al. [1]), which relies on a unit cell approach to represent the GDL as a periodic fibrous micro structure, and assumes:

(1) 3-D repeating basic cell
(2) Steady state one-dimensional heat transfer
(3) Negligible natural convection within basic (unit) cell
(4) No radiation heat transfer between neighboring fibers

The additional features introduced here to improve the generality and physical representation of a GDL structure are:

(5) Statistical distribution of the angles between fibers in two adjacent layers: average value of the angles and their deviations from the average value
(6) Characteristic fiber spacing aspect ratio for various GDL types

Our aim is to present a statistical unit cell approach by modifying the Sadeghi et al.'s model from the geometrical modeling point of view to extend its applicability to a broader range of GDL types, and to use the model to investigate the effects of the geometrical parameters on the thermal conductivity. Detail development of the Sadeghi et al.'s model can be found elsewhere [1] and the focus here will be mainly on the improvements to that model, more specifically (i) the determination of the GDL geometrical properties (parameters) and (ii) the statistical implementation of these parameters into the unit cell model.

In general, unit cell models are based on one unit (basic) cell repeated through the entire medium [1,13]. In the case of a fibrous porous material consisting of layers of fibers, such as most "paper" types of GDLs, a simple, still comprehensive, geometrical model, like the one shown in Fig. 1, seems to capture the essential features. In this figure, $l$ and $w$ are the distance between fibers in the $x$ and $y$ directions, $d$ the fiber diameter, and $\theta$ the angle between fibers in two adjacent layers. The porosity ($\varepsilon$) of the unit cell is a function of all these geometrical parameters, as given in Ref. [1]:

$$\varepsilon = 1 - \frac{\pi d}{8}\left(\frac{l + \frac{w}{\cos(\theta)}}{lw}\right) \tag{1}$$

In principle, the unit cell model consists of mechanical and thermal models [1,13–18] applied to the defined unit cell [1,13]. Ultimately, using Fourier's law of heat conduction and the concept of total thermal resistance network, the effective thermal conductivity can be obtained ($k_{\text{eff}}$) as a function of the geometrical parameters, i.e., $k_{\text{eff}} = f(\varepsilon,\theta,d,\text{l},\text{w})$ The thermal resistance network for the unit cell consisting of the top and bottom blocks is represented in Fig. 2. The unit-cell thermal model is identical to that of Sadeghi et al. [1] and the equations of the model are summarized in Table 1.

### 2.1. Measurement of geometrical parameters

Fibrous porous media such as GDLs can have different structure and geometry in terms of angle distribution, aspect ratio, and fiber diameter. These parameters can generally vary independently of

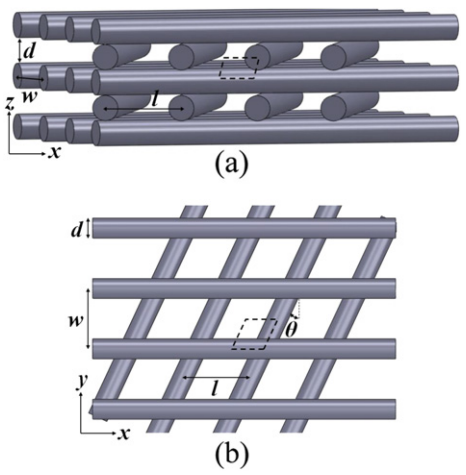


**Fig. 1.** Front isometric view (a) and top view (b) of the geometrical model of GDL (the dashed parallelograms show the unit cell).

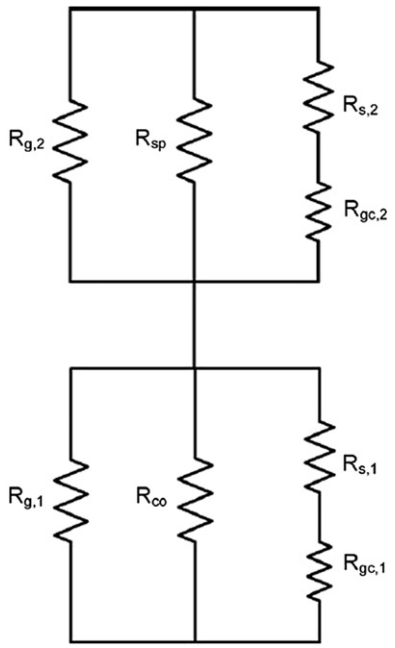


**Fig. 2.** Thermal resistance network for the top and bottom blocks of the unit cell [1].

porosity, and it is *a-priori* necessary to take them into account in geometrical modeling targeted at transport property estimation. In order to do so, we need to have a detailed description of the relevant micro structural parameters for each type of GDL. Such data can be measured optically by a microscope or by other methods, as discussed in the following sub-sections.

*2.1.1. Fiber angle distribution*

In the model of [1], the angles between fibers are assumed to be equal, typically with a set at the mean value of zero. In fact, a distribution of angles exists, as can be readily seen in GDL images. Individual angles can be measured optically (Fig. 3) and a probability distribution can be obtained using statistical methods.

In this study, the angle distribution for two commonly used GDLs, Toray and Sigracet (SGL 25AA), have been optically measured and the corresponding distributions are shown in Fig. 4a and b. The peak probability occurs close to 0° ($\theta = 0$; orthogonal arrangement) and the probability of angles larger than $\theta = 70°$ is low, especially for the SGL GDL. In fact, in the SGL GDLs, the bell curve is more pronounced with higher probabilities of angles close to the orthogonal arrangement.

The statistical distributions were calculated using the statistical software Easyfit [19], and can be approximated by a Gaussian (Normal) distribution in a $-\pi/2$ to $\pi/2$ scale and/or a Beta distribution in a $0-\pi/2$ scale for the Toray GDL (Fig. 4a). A similar but not identical trend can be seen for the SGL GDL (Fig. 4b). Note that, in general, the angles between two fibers in two neighboring layers can take any value from 0 to 90°, yet Fig. 4a and b is plotted using a $-\pi/2$ to $\pi/2$ scale by considering the supplementary angles, hence resulting in a pseudo Normal distribution. In the thermal model calculations, the Beta distribution ($0-\pi/2$ angle scale) should be used.

Having measured the angles, the main question that remains is how to apply such a large number of data to the model. Based on the work carried out by Bahrami et al. [20] on the pressure drop of rough micro-tubes, an analogous correction factor or deviations from the average of the angles is introduced. The average value ($\bar{\theta}$) and the statistical distribution of the deviations from the average value ($p = \theta - \bar{\theta}$) can be obtained from the measured distribution. For any quantity of interest, in this case the effective thermal conductivity, a correction factor corresponding to the deviation of that quantity from its average value can be calculated using:

$$M^* = \frac{M_{cor}}{M_{ref}} = \frac{\int_a^b M\left(\bar{\theta}+p\right)F(p)\mathrm{d}p}{M\left(\bar{\theta}\right)} \tag{22}$$

where $M$ is an arbitrary quantity, $M_{ref}$ and $M_{cor}$ are respectively the reference and corrected (overall) values of $M$, and $F(p)$ is the statistical distribution of variable $p$ ($a \le p \le b$), obtained from the measured angles.

The corrected (overall) values of each quantity ($M_{cor}$) can also be calculated in a simpler way by

$$M_{cor} = \sum_{i=1}^{N} M(\theta_i)P(\theta_i) \tag{23}$$

where $P(\theta_i)$ represents the occurrence probability of an angle with the value of $\theta_i$, and $N$ is the number of the measured angles. In fact, $P(\theta_i)$ acts as a weighting factor for $M(\theta_i)$, the value of property $M$ corresponding to the angle $\theta_i$.

*2.1.2. Aspect ratio ($AR = l/w$)*

The distance between fibers or aspect ratio affects the heat transfer paths as well as the number of contact points between adjacent layers of fibers in a fibrous medium, and is therefore expected to have a noticeable effect on thermal conductivity. However, to the authors' best knowledge, this important parameter has been overlooked in existing heat transfer analyses on fibrous porous media. All the previous works based on the unit cell approach for the calculation of either thermal conductivity [1] or permeability [21,22], considered unity aspect ratio (equal distance between fibers in the $x$ and $y$ directions, see Fig. 5). Here, for the first time, two approaches are presented for determining the aspect ratio in GDLs. The first is, in principle, similar to the method used for measuring the fiber angles, i.e., optical measurements. The other is based on the average pore diameter of each GDL obtained by Mercury Intrusion Porosimetry (MIP) measurements. For a given porosity, $l$ and $w$ are related through the porosity Eq. (1). The common idea in both approaches is to find a second relationship between $l$ and $w$ and then, solve it simultaneously with Eq. (1), to obtain the values of $l$ and $w$ and, subsequently, their ratio (AR).

*2.1.2.1. Optical measurement of aspect ratio.* A sufficient number of areas enclosed between different fibers that are in two neighboring layers (see Fig. 5) can be measured optically, and their average ($A_{ave,m} = \sum_{i=1}^{N_A} A_i/N_A$) can be considered equal to the gap area between the fibers in two neighboring layers:

$$A_{ave,m} = (l-d)(w-d) \tag{24}$$

From the measured data of $A_i$, a statistical distribution of aspect ratio and, in turn, of $l$ and $w$ can also be obtained for each GDL. Figs. 6, 7, and 8 illustrate the statistical distribution of the aspect ratio for GDLs Toray TGP-060, SGL 24AA, and SGL 25AA, respectively. Similarly to estimating the overall value of quantity $M$ from the angle distribution, i.e., Eq. (23), the following equation can be employed for the aspect ratio distribution:

$$M_{cor} = \sum_{k=1}^{N_A} M(\mathrm{AR}_i)P(\mathrm{AR}_i) \tag{25}$$

where $P(\mathrm{AR}_i)$ represents the occurrence probability of an aspect ratio with the value of $\mathrm{AR}_i$, and $N_A$ is the number of the measured

**Table 1**
Equations of the unit cell model [1].

| Parameter | Equation, number |
|---|---|
| Minor relative radii of contact curvature | $\rho'' = \frac{d}{\sqrt{2(1-\cos(2\theta))+2}}$ (2) |
| Major relative radii of contact curvature | $\rho' = \frac{1}{(4/d - 1/\rho')}$ (3) |
| Integral function of $(\rho'\rho''^{-1})$ | $F_1 = \frac{19.1\sqrt{\lambda}}{1+16.76\sqrt{\lambda}+1.34\lambda}$, (4) |
| | $\lambda = \rho'/\rho''$ (5) |
| Maximum force on each contact point | $F_{max} = \frac{P_{GDL} lw}{4}$ (6) |
| Effective elastic modulus | $E' = \left(\frac{1-v_1^2}{E_1} + \frac{1-v_2^2}{E_2}\right)^{-1}$ (7) |
| Major semi axis of elliptical contact | $a = b\left(\frac{\rho'}{\rho''}\right)^{2/3}$ (8) |
| Minor semi axis of elliptical contact | $b = \left(\frac{\rho''}{\rho'}\frac{3F\sqrt{\rho'\rho''}}{4E'}\right)^{1/3} F_1$ (9) |
| Solid thermal accommodation parameter | $\alpha_s = \exp\left[-0.57\left(\frac{T_s-273}{273}\right)\right]\left(\frac{1.4M_g}{6.8+1.4M_g}\right) + \frac{2.4\left(\frac{M_g}{M_s}\right)}{\left(1+\frac{M_g}{M_s}\right)^2}\times\left\{1-\exp\left[-0.57\left(\frac{T_s-273}{273}\right)\right]\right\}$ (10) |
| Thermal accommodation parameter | $\alpha = \left(\frac{2-\alpha s}{\alpha s}\right)+1$ (11) |
| Fluid property parameter | $\beta = \frac{2\gamma}{\Pr(\gamma+1)}$ (12) |
| Mean free path of gas molecules | $\Lambda = \Lambda_{g,\infty}\left(\frac{T_g}{T_{g,\infty}}\right)\left(\frac{P_{g,\infty}}{P_g}\right)$ (13) |
| Gas thermal resistance of bottom block | $\frac{1}{R_{g,1}} = k_g\left(\frac{l\left(w-\frac{d}{2}\right)}{2\left(\frac{d}{2}+\alpha\beta\gamma\right)}\right)$ (14) |
| Gas filled gap thermal resistance of bottom block | $\frac{1}{R_{gc,1}} = k_g\left(\frac{l}{2}\right)\left(\frac{2\alpha\beta\gamma}{\sqrt{(\alpha\beta\gamma)^2-1}}\tan^{-1}\left(\sqrt{\frac{\alpha\beta\gamma+1}{\alpha\beta\gamma-1}}\right)\right)$ (15) |
| Gas thermal resistance of top block | $\frac{1}{R_{g,2}} = k_g\left(\frac{w}{2}\right)\frac{\left(\frac{l}{2}-\frac{d/2}{\cos(\theta)}\right)}{d/2+\alpha\beta\gamma}$ (16) |
| Gas filled gap thermal resistance of top block | $\frac{1}{R_{gc,2}} = \frac{k_g\left(\frac{w}{2}\right)}{\cos(\theta)}\left(\frac{2\alpha\beta\gamma}{\sqrt{(\alpha\beta\gamma)^2-1}}\tan^{-1}\left(\sqrt{\frac{\alpha\beta\gamma+1}{\alpha\beta\gamma-1}}\right)\right)$ (17) |
| Spreading/constriction resistance & modulus of elliptic integral | $R_{sp}$ or $R_{co} = \frac{1}{2\pi ka}\int_0^{\frac{\pi}{2}}\frac{dt}{\sqrt{1-\eta^2\sin^2 t}}$, (18) |
| | $\eta = \frac{1}{\sqrt{1-(b/a)^2}}$ (19) |
| Total thermal Resistance | $R_{tot} = \left[\frac{1}{R_{g,1}}+\frac{1}{R_{gc,1}}+\frac{1}{R_{co}}\right]^{-1} + \left[\frac{1}{R_{g,2}}+\frac{1}{R_{gc,2}}+\frac{1}{R_{sp}}\right]^{-1}$ (20) |
| Effective thermal conductivity | $k_{eff} = \frac{4d}{lwR_{tot}}$ (21) |

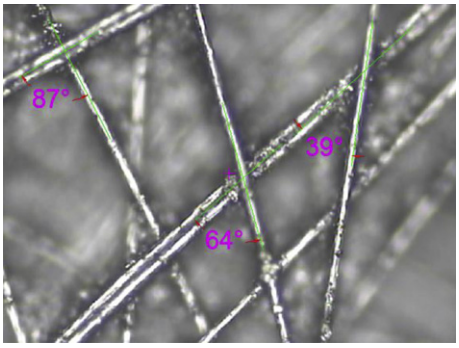


**Fig. 3.** Angles between fibers measured optically (SGL).

aspect ratios and, in fact, the number of $A_i$. In any case, the final value of $M_{cor}$ will generally be an average of the two values of $M_{cor}$ obtained from Eqs. (23) and (25).

*2.1.2.2. Aspect ratio determination from MIP data.* For many of the commonly used GDLs, such as the ones considered in this study, the pore diameter size has been previously reported in the open literature for permeability or other porous media calculations. The pore volume in the unit cell should be the same as the average of the pore volumes inside the GDL of interest, and which can be obtained from MIP measurements. Considering the equivalent diameter of the pore in the MIP method [23,24], the following relationship between the distance between fibers in the $x$ and $y$ directions, $l$ and $w$, can be written:

$$\frac{\pi d_{p,ave}^2}{4} = (lw\varepsilon) \tag{26}$$

With a prescribed porosity, solving this equation, or Eq. (24), simultaneously with the porosity equation of the unit cell, Eq. (1), yields the two unknowns $l$ and $w$ and, therefore, their ratio. Note that the statistical distribution of the aspect ratio in the case of MIP can be obtained from the data of the pore size distribution. The average values of the aspect ratio for some well-known GDLs obtained from MIP [25–32] and the optical approach are listed in Table 2.

It is worthwhile to mention that either of these two methods, optical or MIP, has advantages and drawbacks. The MIP method gives the pore diameter based on volumetric measurements (pores in all the layers) whereas the optical approach is based

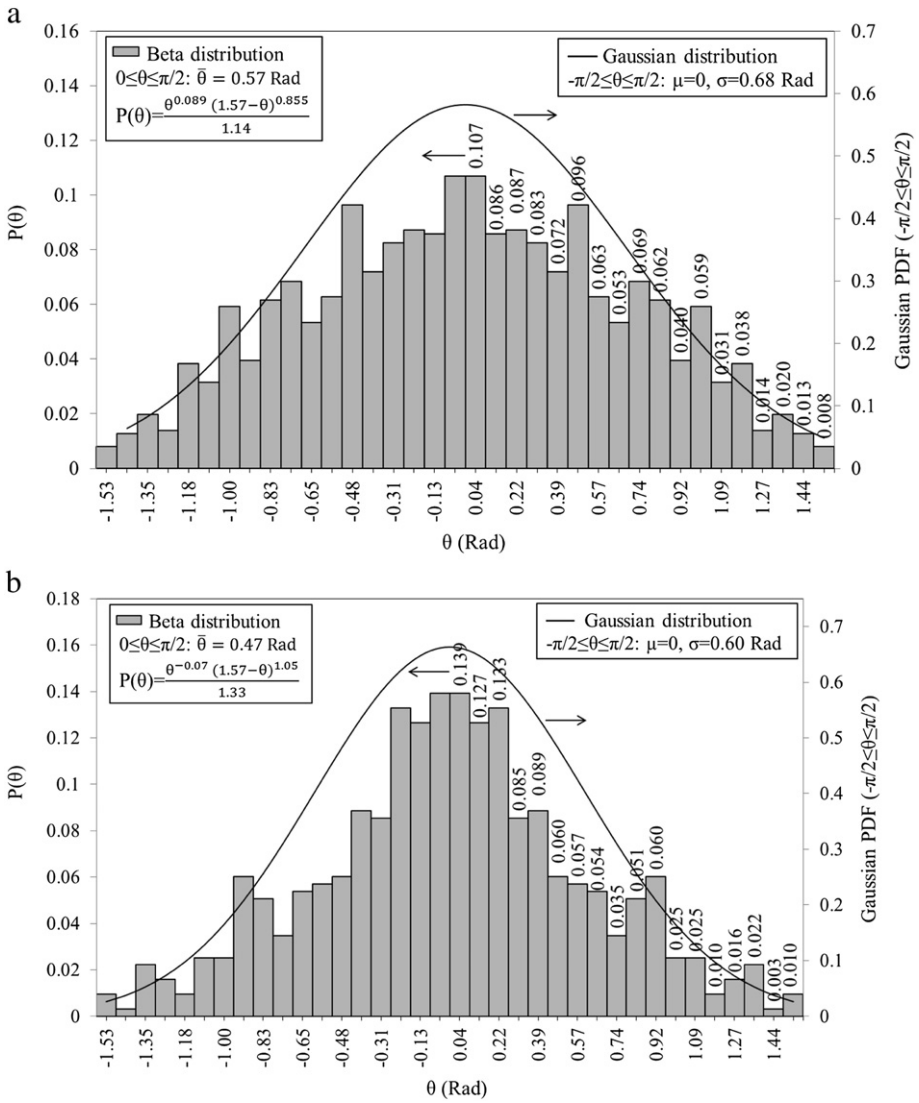


**Fig. 4.** a: Angle distribution of Toray TGP-060. b: Angle distribution of SGL (25AA).

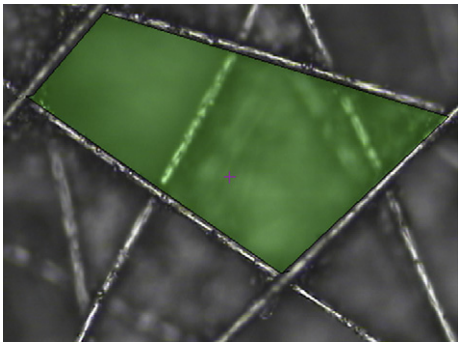

**Fig. 5.** Measurement of the gap area between fibers as optical measurement of aspect ratio.

on gap area measurements in some upper and lower layers of a GDL. The MIP method uses an equivalent circular cross-section assumption for the gap area, which is not accurate. In addition, for the case of treated GDLs, the contact angle of mercury with carbon fibers is not exactly the same as that with PTFE and/or Micro Porous Layer (MPL). Consequently, the optical approach might be more appropriate for thin, treated GDLs, such as most of the Sigracet ones.

*2.1.3. Fiber diameter*

The diameter of fibers can be optically measured as well and a statistical distribution can also be given for this geometrical parameter. However, such measurements are not necessary since considering an average value for fiber diameter is sufficient for the purpose of accurate thermal conductivity modeling, as discussed subsequently. The average fiber diameters measured in this study for the Toray and SGL GDLs are 8.5 and 7.5 μm, respectively.

## 3. Results and discussion

Having determined the geometrical parameters of each GDL and a method to apply them to the model, we can proceed to calculate the through-plane thermal conductivity. A code was written in MATLAB environment to facilitate the $k_{eff} = f(\varepsilon,\theta,d,l,w)$ parametric studies. Note that the present analysis doesn't consider the impact of PTFE in treated GDL. Because of the resistance component-by-component nature of the unit cell approach, it will not be difficult to add the effect of PTFE and MPL (treated GDLs) to the present model in the future, but this requires more information and will be taken into account in future research.

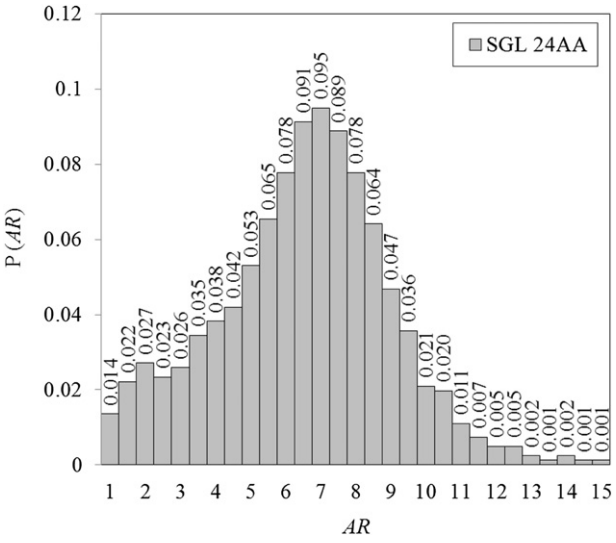


**Fig. 7.** Statistical distribution of the aspect ratio for SGL 24AA.

### 3.1. Fiber angle

As noted earlier, each type of GDL has its own micro structure, and thus a different fiber angle distribution. By plugging the angle statistical distribution (0–π/2 scale) into the correction factor relation, Eq. (22), one can calculate the thermal conductivity corrected based on the angle distribution. In a simpler way, independent of the type of statistical distribution, the overall thermal conductivity can be estimated by Eq. (23).

*3.1.1. Thermal resistance correction factors*

From the angle distribution, one can find the average value (see Fig. 4a and b) and also the correction factors for the deviation of all the possible angles from this average. The values of the correction

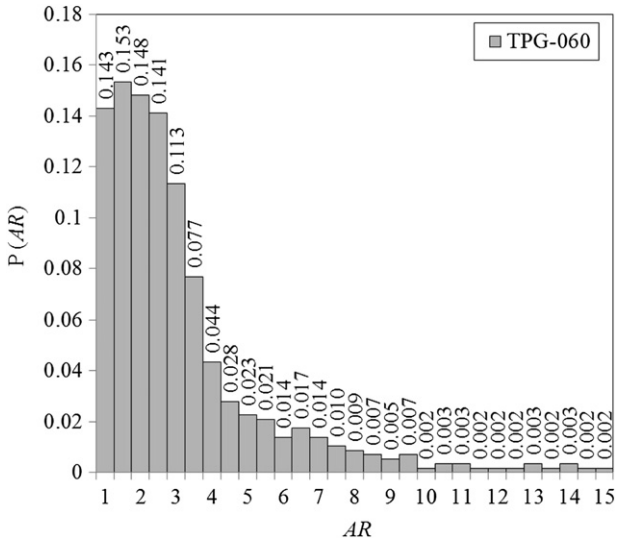


**Fig. 6.** Statistical distribution of the aspect ratio for TGP-060.

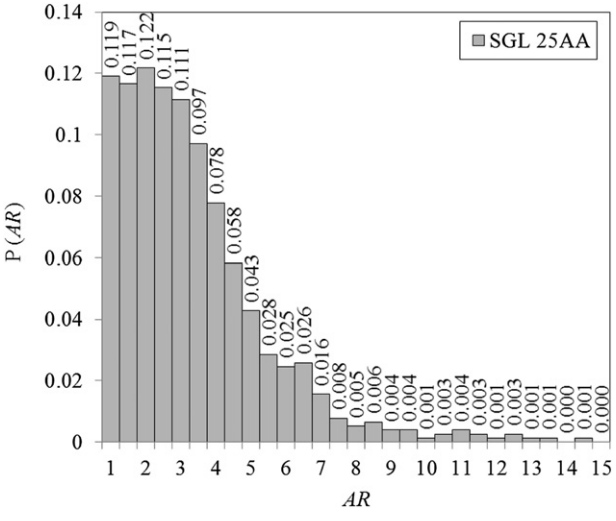


**Fig. 8.** Statistical distribution of the aspect ratio for SGL 25AA.

**Table 2**
Average aspect ratios and some relevant specifications for the well-known studied GDLs.

| Quantity GDL | Porosity (%) | Average pore diameter (μm) | Aspect ratio (−) | |
|---|---|---|---|---|
| | | | MIP | Optical |
| Toray 060 | 78 | 39 [25] | 3.9 | 2.8 |
| Toray 090 | 78 | 33 [26,27] | 2.8 | – |
| Toray 120 | 78 | 28 [28,29] | 2 | – |
| SGL 24AA | 88 ± 0.5 | 66 [26,28,30] | 8 | 6.9 |
| SGL 25AA | 92 ± 0.5 | 60 [26,31] | 2.6 | 3.4 |

factors for thermal resistance components of each GDL are given in Table 3. Note that the correction factors for gas resistances of the top block are always unity since they are not dependent on fiber angle (see Eqs. (14) and (15) in Table 1); hence they are omitted in Table 3. As shown in Table 3, the gas thermal resistance correction factor $R_{gc2}$, unlike the other gas resistances, is significant and seems to be the most sensitive with respect to the angle distribution. Finally, the most important (controlling) factors are related to the spreading/constriction resistances, which are close to unity. In fact, these correction factors show the deviation of each angle from the average value for each GDL. It should be noted that the gas resistances are so large (compared to the other resistances) that heat transfer takes place preferentially and almost exclusively through the solid matrix, even though this entails another large resistance (spreading/constriction resistance) which is still much less than the gas resistances themselves. As a result, the gas thermal resistances do not have any noticeable impact on the through-plane thermal conductivity compared to the solid resistances.

### 3.1.2. Thermal resistance and thermal conductivity dependency on fiber angles

The angle between two fibers determines the area of the contact spot, which, indeed, affects the thermal contact resistance, i.e. spreading/constriction resistance. The dependency of the ratio of spreading/constriction to the total resistance is shown in Fig. 9. The functional dependency is not simple and the contribution of the spreading/constriction resistance is always more than 50%, which indicates the importance of this resistance compared to the other ones.

Fig. 10 depicts the variation of the thermal conductivity with aspect ratio for different fiber angles. The general trend of decreasing thermal conductivity with increasing angle at lower aspect ratios, is reversed at higher aspect ratios, and the aspect ratio at which the switch occurs varies from about 3 for small angles (near-orthogonal fibers) to about 6 for the larger angles (near parallel). As noted earlier, the spreading/constriction resistance is the largest contribution to the total thermal resistance, especially at higher aspect ratios (compared to unity). At aspect ratios close to unity at which the thermal conductivity curves peak, the contribution of the spreading/constriction resistance is the lowest.

Another interesting and important point to note with respect to the manufacturing process is related to the maximum value of thermal conductivity occurring at zero angle ($\theta = 0$), which corresponds to the orthogonal arrangement of fibers. If we connect the maximum points, a second-order polynomial can be used to correlate the maximum effective thermal conductivity in terms of the fiber angle ($\theta$) (for each specified porosity and diameter). This indicates that the dependency of the *maximum* thermal conductivity on fiber angles is relatively simple, especially for the typical range of fiber angles ($0 \le \theta \le \pi/3$). Examination of Fig. 10 shows that in this range of angles, the maximum thermal conductivity is essentially independent of aspect ratio. It would be very interesting to perform similar studies on the in-plane and electrical conductivity, as well as permeability and diffusivity, to identify the optimal fiber angle for GDLs.

**Table 3**
Typical values of correction factors for thermal resistance components of two well-known GDLs.

| GDL | Thermal resistance correction factors | | | |
|---|---|---|---|---|
| | $R^*_{sp}$ | $R^*_{g,2}$ | $R^*_{gc,2}$ | $R^*_{tot}$ |
| Toray 060 | 1.06 | 0.94 | 1.41 | 1.03 |
| SGL 25AA | 1.12 | 0.95 | 1.49 | 1.09 |

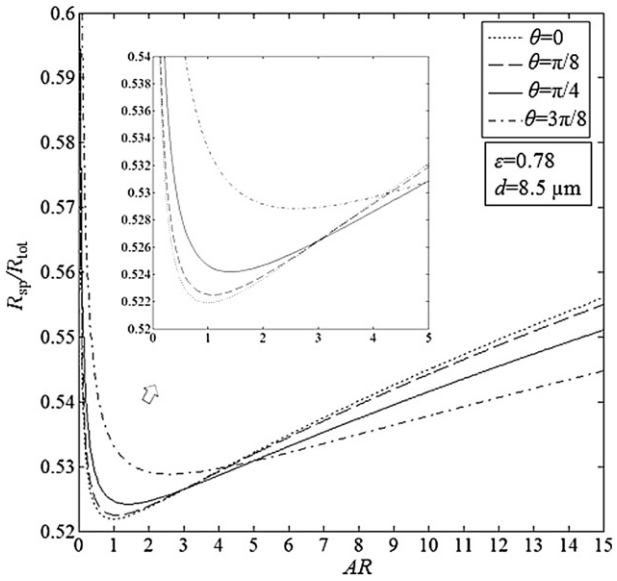


**Fig. 9.** Dependency of spreading/constriction resistance on angle for GDLs.

### 3.2. Fiber diameter

The changes in thermal conductivity for different fiber diameters are shown in Fig. 11 at different aspect ratios. Both thermal

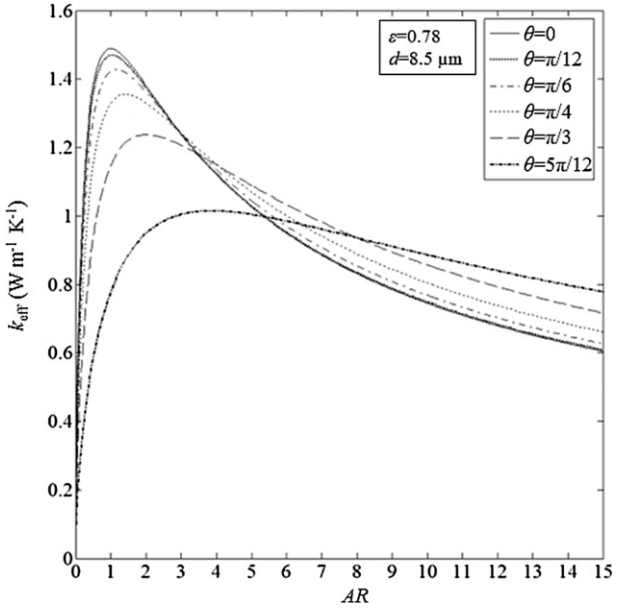


**Fig. 10.** Dependency of thermal conductivity on angle for GDLs.

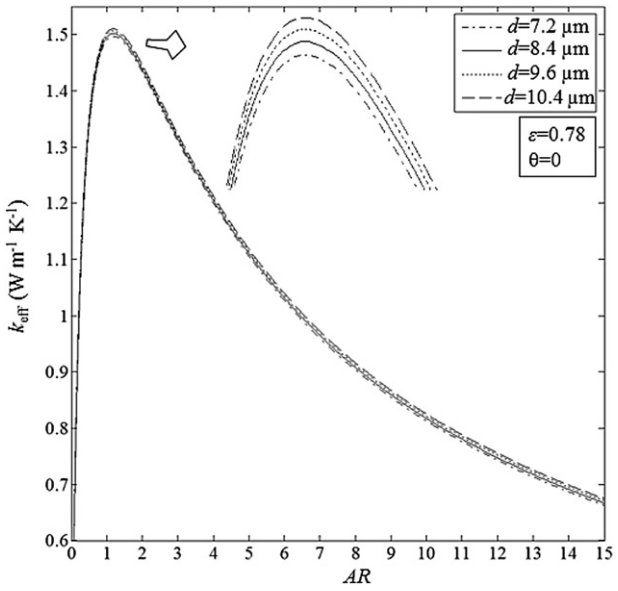


**Fig. 11.** Effect of diameter on through-plane thermal conductivity of GDLs.

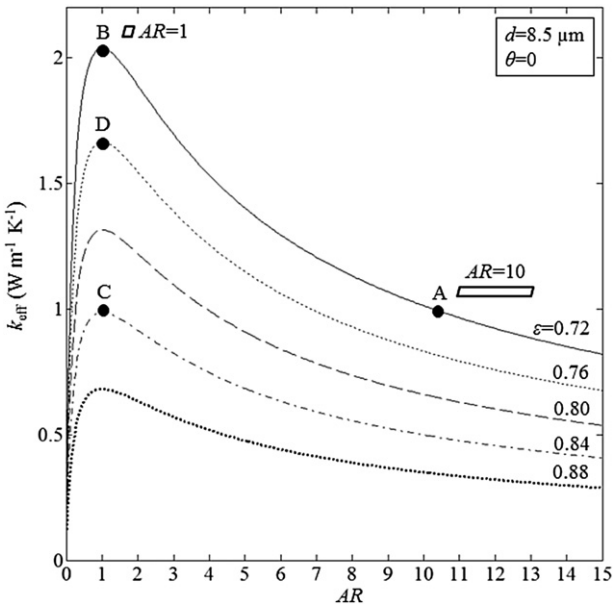


**Fig. 12.** Effect of aspect ratio on through-plane thermal conductivity of GDLs with different porosities (the parallelograms shown on the figure represent the AR for the unit cell).

conductivity and its maximum value are virtually independent of the fiber diameter throughout the range of investigated porosities and aspect ratios. This suggests that the fiber diameter can be manipulated for increasing other transport properties such as permeability without incurring any penalty in the through-plane thermal conductivity. In fact, increasing the fiber diameter not only increases the thermal conductivity, even though slightly, but also enhance permeability significantly [21,22]. In practice, the maximum thermal conductivity does not vary with aspect ratio and fiber diameter ($k_{\text{eff max}} \neq f(d,AR)$).

### 3.3. Aspect ratio

One of the most important geometrical parameters of fibrous porous materials is the aspect ratio. The impact of this parameter can be as important and effective as porosity, as it can be manipulated to achieve the desired transport properties for different purposes. Fig. 12 represents the thermal conductivity as a function of the two important parameters, aspect ratio and porosity. The dependency of thermal conductivity on porosity is not as complex as for angle. Fig. 12, similarly to Fig. 11, depicts a maximum at an aspect ratio very close, but not necessarily equal, to unity, for each value of porosity. At specified values of $\theta$ and $d$ (real case), interestingly enough, the maximum thermal conductivity, $k_{\text{eff max}}$, is practically independent of the aspect ratio. This can be very important for GDL manufacturing. For a given type of GDLs $d$ and $\theta$ are usually fixed, and as a result, it would be sufficient to account for $k_{\text{eff max}}$ as a function of porosity only; i.e., $k_{\text{eff max}} = f(\varepsilon)$. Connecting the maximum points in the cases shown in Fig. 12, a *linear* relation is obtained in the form of:

$$k_{\text{eff max}} = -8.48\varepsilon + c \tag{27}$$

where the value of the constant $c$ is depends on $\theta$ (and $d$) (e.g., for $\theta = 0$ ($d = 8.5$ μm); then $c = 8.13$). For the typical range of the fiber angles in GDLs, that is, $0 \leq \theta \leq \pi/3$ (see Fig. 4a and b), the maximum thermal conductivity is practically independent of the aspect ratio (Fig. 10, also see Figs. 11 and 12). As a result, $k_{\text{eff max}}$ can practically be considered as a function of only two geometrical parameters; $\varepsilon$ and $\theta$.

It should be noted that an aspect ratio of unity corresponds to the square arrangement, which results in the highest through-plane thermal conductivity. However, other transport properties such as in-plane thermal conductivity, permeability, diffusivity, and electrical conductivity have to be considered as well. A multi-parameter optimization of such properties with respect to the geometrical parameters is ultimately required to determine an optimum structure of a GDL for better water and heat management of fuel cells. It should also be noted that production of optimally designed arrangements such should become possible as precise control of fiber orientations and arrangements during fabrication of fibrous media is becoming more practical with progress in manufacturing technology.

Fig. 12 provides a helpful illustration of the importance of the aspect ratio in comparison to the primary parameter characterizing a porous medium, i.e., porosity. It is obvious that with increasing porosity (at fixed values of aspect ratio), the thermal conductivity decreases whereas the permeability increases. As a result, there is a trade-off between the through-plane thermal conductivity and permeability in terms of porosity. For instance, consider points A, B, C, and D on Fig. 12. To increase the thermal conductivity from 1 to 2 W m$^{-1}$ K$^{-1}$ and, in fact, double it, the usual approach that usually comes to mind is to decrease the porosity (e.g., from 0.8 to 0.72, shown in Fig. 12), which may markedly reduce other transport properties such as permeability. Based on the insights and results of this study, one can in fact double the thermal conductivity from point A to point B by only manipulating the aspect ratio and keeping the porosity fixed ($\varepsilon = 0.72$). This example illustrates the strong dependency of the thermal conductivity on the aspect ratio. As explained, points A and B, which are both on the solid curve, have the same porosities ($\varepsilon = 0.72$) but completely different thermal conductivities due to their different aspect ratios.

Conversely, one can keep the through-plane thermal conductivity fixed and increase the porosity or decrease aspect ratio by following any horizontal straight line on Fig. 12 (e.g., from point A to point C). For instance, points A and C have the same thermal conductivities but different porosities and aspect ratios. In terms of the through-plane heat transfer, there is no difference between points A and C. However, point C is preferred, as it corresponds to a higher

porosity and hence higher permeability and less solid (fibers), which can reduce the cost of materials in the manufacturing process. These points might inform GDL manufacturing, as available GDL products usually fall within the regions far from the peak points on Fig. 12. In general, depending on the specific application and the targeted properties, one can keep one or two of the geometrical parameters fixed and adjust the others to achieve an optimal fibrous medium structure.

Finally, we consider points A and D where point D has a higher thermal conductivity with more porosity. Therefore, a fibrous pours medium with higher porosity will not necessarily have a lower thermal conductivity. This interesting conclusion refutes the conventional notion for heat transfer in porous media on which all the other available models have been implicitly based i.e. that the higher the porosity, the less the solid matrix and, therefore, the lower the thermal conductivity.

### 3.4. Model validation

The results of the present model are compared to those of Sadeghi et al. [1] and to available experimental data [33,34] as well as data obtained as part of this work using a thermal conductivity testbed described in detail elsewhere [4–6]. Different types of commonly used GDLs with documented through-plane thermal conductivity (Toray TGP-H-060 to 120 and also SGL 24AA and 25AA) have been selected, and their thermal conductivities were calculated using both models.

As shown in Fig. 13, both models yield reasonable predictions of the thermal conductivity of the untreated Toray GDLs (TGP H-060 and TGP H-090), with overall better agreement of the present model with experiments especially for SGL 24AA which has a high aspect ratio. Note that in Ref. [33] the thermal conductivity measurements were not performed under vacuum conditions (even though some insulation was used), which resulted in small overestimates as pointed out by the authors. Another point to note is that the thermal conductivities measured in Ref. [33] have been obtained from the so-called two-thickness method for TGP-H-060 and TGP-H-090. According to Table 2, the porosities of these two GDLs are the same and their aspect ratios are close to each other.

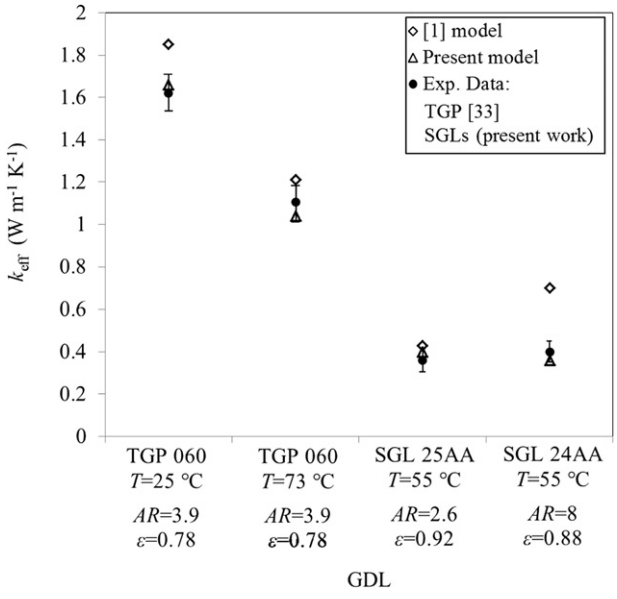


**Fig. 13.** Comparison of the thermal conductivities calculated by the models with experimental data.

**Table 4**
Experimental data of [35] for evaluation of the aspect ratio effect on thermal conductivity for different Torays.

| Type of Toray | $k_{eff}$ (W m$^{-1}$ K$^{-1}$) | | |
|---|---|---|---|
| | Compression pressure (bar) | | |
| | 4.6 | 9.3 | 13.9 |
| TGP-H-060 | 0.41 | 0.53 | 0.66 |
| TGP-H-090 | 0.50 | 0.65 | 0.73 |
| TGP-H-120 | 0.62 | 0.81 | 0.89 |

As a result, the only value of the thermal conductivity obtained for both GDLs TGP-H-060 and -090 by using the two-thickness method can be considered as the average value of their actual thermal conductivities.

We also implemented both models at another temperature, i.e., 73 °C, for which experimental data is also available. The comparisons indicate that both models account well for the effect of temperature on effective thermal conductivity.

Some thermal conductivity data measured under different conditions have been reported in [35,36] for each of the treated Torays TGP-H-060, 090, and 120 (5% PTFE) and presented separately in Table 4. Based on the observation that the changes in the sample–sample contact resistance were low with increasing compression, the authors [35] assumed a negligible thermal contact resistance between two samples. However, the relative independence on compression pressure does not necessarily indicate that contact resistance is negligible. Nevertheless, the data of [35] can still be used for the purpose of qualitative comparisons between the considered Toray papers. The measured data in Table 4 show a reduction in the thermal conductivity from TGP-H-120 to TGP-H-060 at all compressive loads. This interesting reduction trend can now be explained by the effect of the aspect ratio parameter; with increasing the aspect ratio from TGP-H-120 to TGP-H-060 (see Table 2), the effective thermal conductivity decreases. This trend cannot be explained or justified by other models. Finally, we consider SGL 24AA and 25AA to further investigate the effect of the geometrical parameters on the thermal conductivity. As shown in Fig. 13, the models have markedly different estimates for SGL 24AA. The present (statistical) model improves the prediction significantly compared to the previous model [1] which is based on a unity aspect ratio and a homogeneous GDL with zero value of angle (orthogonal arrangement of fibers).

The experimental data also indicates that the thermal conductivities of two SGLs 24AA and 25AA with completely different porosities are almost the same, and this again can be explained by the results of the present study. The porosity of SGL 24AA is 0.88, which is higher than that of SGL 25AA, i.e., 0.92. This might erroneously lead to the expectation that SGL 24AA would have a higher thermal conductivity because of its lower porosity. However, the increase in conductivity arising from the lower porosity of SGL 24AA is offset by the higher aspect ratio compared to SGL 25AA. This can be considered as experimental evidence of the physical realism of the present model, as points A and C on Fig. 12 qualitatively correspond to the real cases of SGL 24AA and 25AA, respectively.

## 4. Conclusion

A statistical unit cell model was proposed for estimating the through-plane thermal conductivity of GDLs, which considers not only porosity, but also other geometrical properties such as angle distribution and aspect ratio. The geometrical parameters of a GDL structure, their effects on through-plane thermal conductivity, and how to measure or determine them for different types of GDL were

discussed in detail. These parameters were determined for several types of commonly used GDLs. The aspect ratio was found to be as important as porosity in determining conduction heat transfer. The results also shed a new perspective on the notion that a fibrous porous medium with higher porosity yields a lower thermal conductivity, and show that it is possible for two fibrous media with the same porosity to have completely different thermal conductivity and vice versa, due to the contributions of other geometrical parameters, especially the aspect ratio. The important insight on the complementary role of aspect ratio provides a rational explanation of some experimental trends and results that were considered contradictory. The results of the model also yield the structure of a GDL providing the maximum through-plane thermal conductivity. It was found that, the *maximum* thermal conductivity is not a function of fiber diameter and aspect ratio ($k_{\text{eff max}} \neq f(d,AR)$) and depends primarily on porosity and fiber angle ($k_{\text{eff max}} = f(\varepsilon,\theta)$).

In general, the concepts and techniques presented in this study can be extended to the determination of geometrical properties of any fibrous porous media, and can be adapted to estimate other GDL transport properties such as permeability. The insights gained through this work can open alternative avenues for tailoring and optimizing the geometrical parameters of fibrous porous media from the viewpoint of manufacturing process and transport properties.

## Acknowledgement

The authors gratefully acknowledge the financial support of the Natural Sciences and Engineering Research Council of Canada (NSERC).

## Nomenclature

| Symbol | description unit |
|---|---|
| AR | aspect ratio |
| $a,b$ | major and minor semi axes of elliptical contact m |
| $a,b$ | upper and lower integral bonds (variable $p$) |
| $c$ | constant |
| $d$ | fiber diameter m |
| $d_{p,\text{ave}}$ | average pore diameter m |
| $E$ | Young's modulus Pa |
| $E'$ | effective elastic modulus Pa |
| Exp. | experimental value |
| $F(p)$ | statistical distribution function of variable $p$ |
| $F_1$ | integral function of $(\rho'\rho''^{-1})$ |
| $F_{\max}$ | maximum force on each contact point $N$ |
| GDL | Gas Diffusion Layer m |
| $k_{\text{eff}}$ | effective thermal conductivity W m$^{-1}$ K$^{-1}$ |
| $l$ | distance between two fibers in the $x$ direction m |
| $M$ | arbitrary quantity |
| MIP | Mercury Intrusion Porosimetry |
| MPL | Micro Porous Layer |
| $M_g$ | gas molecular weight g mol$^{-1}$ |
| $M_s$ | solid molecular weight g mol$^{-1}$ |
| $N$ | number of data |
| $N_A$ | number of the measured areas between fibers |
| $P$ | probability |
| PDF | probability density function |
| PTFE | polytetrafluoroethylene |
| $p$ | random variable (deviation from the average value) |
| $P_{\text{GDL}}$ | GDL pressure Pa |
| Pr | Prandtl number |
| $R$ | thermal resistance K W$^{-1}$ |
| $R_{\text{co}}$ | constriction resistance K W$^{-1}$ |
| $R_{\text{sp}}$ | spreading resistance K W$^{-1}$ |
| $T$ | Temperature K |
| $w$ | distance between two fibers in the $y$ direction m |

*Greek letter*

| | |
|---|---|
| $\alpha$ | thermal accommodation parameter |
| $\mu$ | mean (Gaussian distribution) |
| $\beta$ | fluid property parameter |
| $\gamma$ | heat capacity ratio |
| $\varepsilon$ | porosity |
| $\eta$ | modulus of elliptic integral |
| $\theta$ | angle between two fibers Rad |
| $\overline{\theta}$ | average value of the measured angles Rad |
| $\lambda$ | ratio of relative radii of curvature $(\rho'\rho''^{-1})$ |
| $\rho', \rho''$ | major and minor relative radii of curvature m |
| $\sigma$ | standard deviation (Gaussian distribution) |
| $\upsilon$ | Poisson's ratio |
| $\Lambda$ | mean free path of gas molecules m |
| $s$ | solid (carbon fiber) |

*Subscript*

| | |
|---|---|
| 1 | bottom block of the unit cell |
| 2 | top block of the unit cell |
| $\infty$ | standard condition state |
| ave | average value |
| cor | corrected value |
| eff | effective (overall) value |
| $g$ | gas |
| gc | gas filled gap |
| $i$ | $i$-th component of a set of variables or summation index |
| $m$ | measured |
| max | maximum value |
| ref | reference value |
| tot | total |

*Superscript*

| | |
|---|---|
| * | correction factor |

## References

[1] E. Sadeghi, M. Bahrami, N. Djilali, J. Power Sources 179 (2008) 200–208.
[2] J.B. Chaitanya, T.T. Stefan, J. Power Sources 179 (2008) 240–251.
[3] N. Djilali, D. Lu, Int. J. Therm. Sci. 41 (2002) 29–40.
[4] E. Sadeghi, N. Djilali, M. Bahrami, J. Power Sources 196 (2011) 246–254.
[5] E. Sadeghi, N. Djilali, M. Bahrami, J. Power Sources 195 (2010) 8104–8109.
[6] E. Sadeghi, N. Djilali, M. Bahrami, J. Power Sources 196 (2011) 3565–3571.
[7] B. Markicevic, N. Djilali, J. Power Sources 196 (5) (2011) 2725–2734.
[8] N.A. David, P.M. Wild, J. Hu, N. Djilali, J. Power Sources 192 (2009) 376–380.
[9] A. Radhakrishnan, PhD thesis, Rochester Institute of Technology, New York, USA, 2009.
[10] M. Wang, J.H. He, J.Y. Yu, N. Pan, Int. J. Therm. Sci. 46 (9) (2007) 848–855.
[11] J. Ramousse, S. Didierjean, P. Lottin, D. Maillet, Int. J. Therm. Sci. 47 (2008) 1–8.
[12] A. Pfrang, D. Veyret, F. Sieker, G. Tsotridis, Int. J. Hydrogen Energy 35 (2010) 3751–3757.
[13] M. Bahrami, M.M. Yovanovich, J.R. Culham, Int. J. Heat Mass Transfer 49 (2006) 3691–3701.
[14] M. Bahrami, J.R. Culham, M.M. Yovanovich, G.E. Schneider, J. Appl. Mech.-T. ASME 59 (2006) 1–12.
[15] M. Bahrami, M.M. Yovanovich, J.R. Culham, J. Tribol.-T. ASME 127 (2005) 884–889.
[16] M. Bahrami, J.R. Culham, M.M. Yovanovich, J. Thermophys Heat Transfer 18 (2004) 326–332.
[17] M. Bahrami, J.R. Culham, M.M. Yovanovich, J. Heat Trans.-T. ASME 126 (6) (2004) 896–905.
[18] M. Bahrami, M.M. Yovanovich, J.R. Culham, Int. J. Heat Mass Transfer 48 (16) (2005) 3284–3293.
[19] Easyfit Software, MathWave Technology, http://www.mathwave.com/help/easyfit/index.html.
[20] M. Bahrami, M.M. Yovanovich, J.R. Culham, J. Fluid Eng.-T. ASME 128 (2006) 632–637.
[21] A. Tamayol, M. Bahrami, Int. J. Heat Mass Transfer 52 (2009) 2407–2414.
[22] J.T. Gostick, M.W. Fowler, M.D. Pritzker, M.A. Ioannidis, L.M. Behra, J. Power Sources 162 (2006) 228–238.

[23] P.A. Webb, An Introduction to the Physical Characterization of Materials by Mercury Intrusion Porosimetry with Emphasis on Reduction and Presentation of Experimental Data, Micromeritics Instrument Corporation, Norcross, Georgia, 2001.
[24] H.L. Ritter, L.C. Drake, Ind. Eng. Chem. Anal. Ed. 17 (1945) 782–786.
[25] M.F. Mathias, J. Roth, J. Fleming, W. Lehnert, in: W. Vielstich, H.A. Gasteiger, A. Lamm (Eds.), Handbook of Fuel Cells: Fundamentals, Technology and Applications, John Wiley, New York, 2003.
[26] A. El-kharouf, B.G. Polleta, D. Brettb, Effect of Commercial Gas Diffusion Layer (gdl) Properties on pemfc Performance – from Ex-situ Testing to Modelling, www.fuelcells.bham.ac.uk.
[27] P. Cheung, J.D. Fairweather, D.T. Schwartz, J. Power Sources 187 (2009) 487–492.
[28] V. Radhakrishnan, P. Haridoss, Int. J. Hydrogen Energy 35 (2010) 11107–11118.
[29] J. Gostick, M. Pritzker, M. Ioannidis, M. Fowler, J. Electrochem. Soc. 157 (2010) B563–B571.
[30] P. Fluckiger, PhD thesis, ETH, Zurich, Switzerland, 2009.
[31] J. Scholta, M. Schulze, S. Donath, J. Pauchet, S. Fell, G. Tsotridis, T. Damjanovic, 2nd CARISMA International Conference on Progress in MEA Materials for Medium and High Temperature Polymer Electrolyte Fuel Cells, September 19–22, 2010, La Grande Motte, France.
[32] A. Bazylak, D. Sinton, Z.S. Liu, N. Djilali, J. Power Sources 163 (2007) 784–792.
[33] M. Khandelwal, M.M. Mench, J. Power Sources 161 (2006) 1106–1115.
[34] Toray Carbon Paper-manufacturer Data Sheet, http://www.torayca.com/index2.html.
[35] O. Burheim, J.G. Pharoah, H. Lampert, J. Fuel. Cell. Sci. Tech. (2011). http://dx.doi.org/10.1115/1.4002403.
[36] O. Burheim, P.J.S. Vie, J.G. Pharoah, S. Kjelstrup, J. Power Sources 195 (2010) 249–256.